Wall-resolved large eddy simulation in refinery ribbed pipes

By M. Zhu†, E. Riber†, B. Cuenot†, J. Bodart‡ AND T. Poinsot†¶

The turbulent flow in a helically ribbed tube is performed with a large eddy simulation, using a non-slip boundary condition with a resolved boundary layer and a WALE sub-grid scale model to ensure the correctness of the flow near the wall. The impact of ribs on the velocity and pressure fields is investigated, showing a flow acceleration on top of the rib and recirculation zones upstream and downstream of the rib. Turbulence is intensified by the presence of the ribs, but there is no cumulative effect as the inter-rib distance is too large to induce the interaction between two successive rib wakes. Finally, the total pressure loss contribution of pressure drag is largely dominating, whereas it is zero in the smooth tube. These findings provide useful information for future development of roughness-type wall modeling in such configurations.

1. Introduction

Olefins such as ethylene or propylene are produced by thermally cracking gaseous hydrocarbons (ethane, naphtha, natural gas, etc.). The thermal cracking reaction is conducted by introducing both gaseous hydrocarbons and steam in a cracking coil disposed in a furnace where burners provide heat. The mixture is heated to reach cracking temperatures (typically 1200K for ethane) while flowing through the coil at high velocity. Typical bulk Reynolds numbers range from 50,000 to 100,000. The cracking coil is composed of many straight pipes, typically 10 m long, connected together by bends. Fast heating of the mixture inside the coils is a key process for thermal cracking efficiency. However, excessive production of lighter hydrocarbons (e.g. methane, free carbons) may happen if the temperature level is too high. In addition, overly too hot walls induce coke deposit on the internal coil surface, reducing the heat transfer coefficient. To optimize the heat transfer, while keeping the temperature at a reasonable level, a technical solution proposed by coil manufacturers is to take advantage of turbulence and modify the inner pipe surface. By placing fins or ribs (see Figure 1), turbulence is increased thanks to the additional shear layer induced by the rib, leading to more intense mixture stirring between the hot flow near the walls and the colder flow in the center of the pipe, and therefore to faster heating. This process, however, significantly increases the pressure drop in the system, and more mechanical power is required to maintain the same flow rate. An optimum is needed to be found, that makes the best trade-off between process efficiency and operational cost.

Many experimental works (Bergles *et al.* 1974; Sethumadhavan & Raja Rao 1983; Zhang *et al.* 1991; Saha 2010; García *et al.* 2012) may be found on the characterization of the friction factor and heat transfer coefficient in straight ribbed pipes, with various rib shapes, geometry parameters, Reynolds numbers, and fluid properties. From these works,

† CERFACS, France
‡ ISAE/DAEP, ENSICA, France
¶ IMFT CNRS, France

FIGURE 1. Example of internal ribbed pipe geometry (http://www.kubota.com.sa).

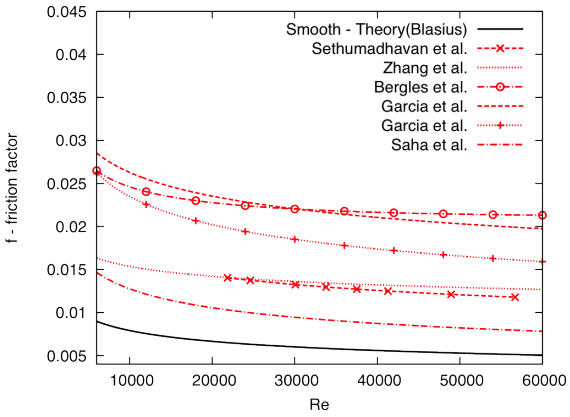

FIGURE 2. Friction factors versus Reynolds numbers in ribbed pipes according to published experimental works.

different semi-experimental formulas for the friction coefficient $f(\mathrm{Re})$ dependent on the rib parameters are proposed. Figure 2 plots the results obtained with these formulas and the rib parameters of the present study. Unfortunately the results are varied and although they all exhibit the same trend, a quantitative estimate of pressure loss is missing. Indeed an increase in only a few percents of selectivity represents a considerable cost, and an accurate estimation of the pressure drop in the ribbed pipe, as well as a quantification of the turbulent flow property changes, compared with that found in a smooth pipe are critical steps toward finding an optimal geometry.

In the present work, Large Eddy Simulation (LES) is used to study the small-scale wall flow dynamics in turbulent ribbed pipes. Because of the complexity of the near-wall flow field, which shows separated and recirculation zones around the ribs, classical wall models would fail to accurately reproduce the wall friction and the inner viscous layer unless the turbulent flow is fully resolved. The present objective is to obtain a validated numerical database of the flow field generated by helical ribs, describing with high accuracy the complex physical mechanisms and flow structure near the walls. Detailed analysis of this database should set the ground for alternative wall-modeling that fully takes into account the rib effect, in a smooth geometrical domain, therefore circumventing the computational cost associated with meshing the rib. This will be crucial for the future LES of large-scale reactor systems in which a fully resolved boundary layer is computationally too expensive.

2. Methodology

Figure 3 displays the ribbed pipe geometry considered in this work. It is a cylindrical tube of diameter $D = 51$ mm in which the helicoidal ribs with a semi-circular shape have been inserted. Ribbed pipes are characterized by the rib height e and the pitch p (axial distance between two ribs), usually expressed with the ratios e/D and p/e. In the present configuration these quantities are $e/D = 0.036$ and $p/e = 11.6$, which are relevant to the targeted petrochemicals applications. The rib height is very small compared with the pipe diameter, thus there is no blocking effect. Thanks to the increased source term S_{qdm} (see definition in Eq. (2.1)), the bulk velocity is unchanged compared with that of a smooth pipe. Following the classification of roughness of Perry *et al.* (1969); Tani (1987),

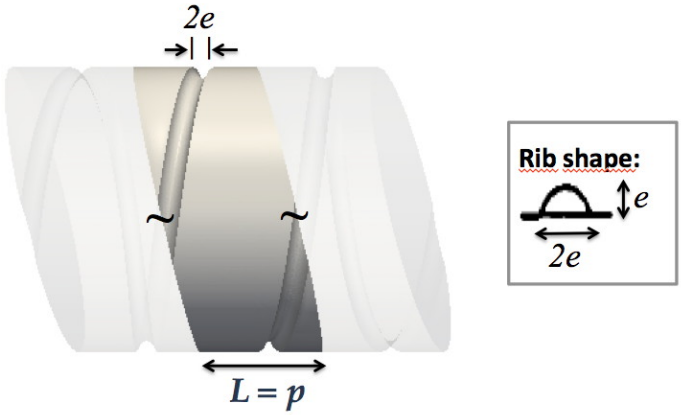

FIGURE 3. Ribbed pipe configuration with details of the ribbed geometry. The dimensions are $p = 21.74$ mm, $e = 1.875$ mm, $D = 51$ mm.

the flow outside the boundary layer stays undisturbed for $p/e < 4$. When p/e exceeds 4, eddies of the size of the roughness height are shed from the roughness elements and penetrate into the bulk flow toward the pipe center. The studied configuration clearly falls in the second category, which is consistent with the objective of increasing turbulent mixing close to the wall.

Air at a constant temperature of 973 K and pressure of 1 bar flows through the pipe at a bulk velocity of $u_b = 62$ m/s, corresponding to a bulk diameter-based Reynolds number $\mathrm{Re} = \rho u_b D/\mu$ of 28000. In a smooth pipe of same diameter, this bulk Reynolds number leads to a friction Reynolds number $\mathrm{Re}_\tau = 770$, i.e. a viscous sublayer ($y^+ < 5$) thickness of about 0.16 mm. Using these values, the rib is of the order of a few tens wall units ($e^+ \sim 50$), and is fully embedded in the viscous layer. It is however too big to allow a direct application of wall laws or friction factor correlations including roughness.

As shown on Figure 3, only one periodic pattern (periodic pipe of length $L = p$) is computed. Prior tests on configurations built using 1, 3, and 5 repeating patterns have shown that the number of computed patterns has little effect on the total pressure drop and are not considered here.

For comparison purposes, the same pipe without ribs (smooth pipe) was also computed with the exact same methodology and conditions, i.e. same bulk Reynolds number and domain length.

To maintain the flow in a periodic configuration, the mean pressure gradient contribution is added under the form of an additional source term S_{qdm} in the axial momentum equation, together with a work contribution uS_{qdm} added to the total energy equation. This source term is directly linked to the global pressure loss, and is a direct estimation of the Fanning friction coefficient f in a smooth pipe as

$$S_{qdm} = \frac{2f\rho u_b^2}{D}, \tag{2.1}$$

where u_b is the bulk velocity. As for the mesh design, and because the total pressure loss in the ribbed pipe is not known *a priori*, the source term is adjusted from preliminary simulations to ensure that the simulated flow reaches the target bulk velocity.

Simulations were all performed with the code AVBP of CERFACS that solves the compressible flow equations on unstructured meshes. Up to third-order in space, fourth-

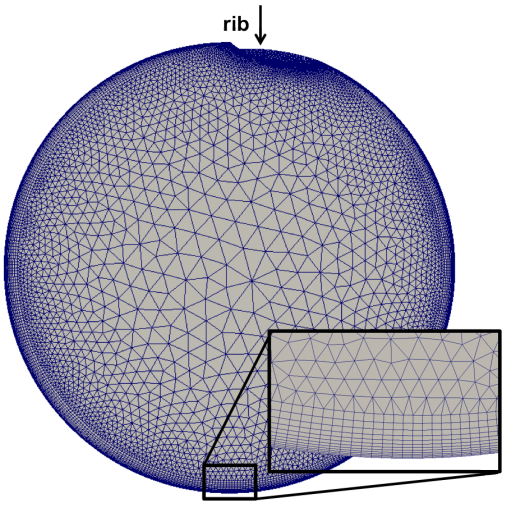

FIGURE 4. View of the computational mesh: transverse cut and zoom in the wall region.

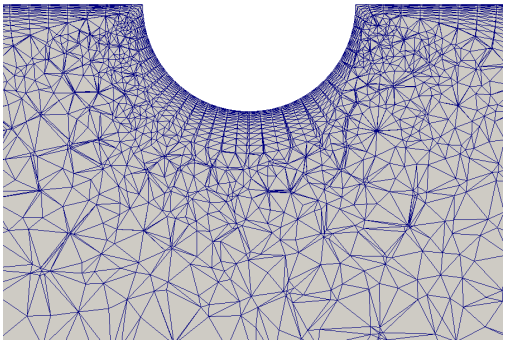

FIGURE 5. View of the computational mesh: axial cut around one rib.

order in time numerical schemes are available (Colin & Rudgyard 2000). Figure 4 shows the mesh used for the computation: the mesh is refined close to the wall, down to $y^+ = 1$ where y^+ is the distance from the wall to the closest node in wall units. This ensures a full resolution of the viscous layer. Because neither the friction velocity nor changes along the ribbed wall were known *a priori*, preliminary simulations were run to gradually adapt the mesh size to the $y^+ = 1$ constraint. Note that a hybrid mesh is used, with tetrahedra in most of the domain and a thin layer of prisms along the wall (Figure 5). This allows a better control of y^+ and improved behavior of the numerical scheme in the wall region. The mesh is significantly coarsened toward the pipe center, where it corresponds to a typical LES resolution. Periodic boundary conditions are applied in the axial direction, while the wall is simply no-slip adiabatic. The correctness of the sub-grid scale model behavior in the vicinity of the wall is ensured through the use of the WALE sub-grid scale model (Ducros *et al.* 1999).

The final mesh contains 2.22 million cells (800706 nodes), leading to a computing time of 105 CPUh for one flow-through time. The simulation was run on 192 cores of the Bull B510 supercomputer of CERFACS, for 540 flow-through times L/u_b (approximately 190 ms), and statistics were collected during 160 ms (450 flow-through times).

3. Results

3.1. *Velocity*

Figure 6 shows a snapshot of a Q-criterion isosurface in two periodic patterns, colored by the direction of axial velocity component (positive=white; negative=black). Flow in the tube is from left to right, and the same for all figures. As expected, the flow appears highly turbulent with elongated vortical structures in the wall region. Recirculating flow is visible downstream the ribs and the turbulence intensity seems slightly higher behind the ribs. The mean axial velocity field is presented in Figure 7, in both transverse (Figure 7 (a)) and axial (Figure 7 (b)) cut planes. The mean axial flow appears generally axisymmetric, except close to the wall where a persistent recirculation zone is observed, starting just

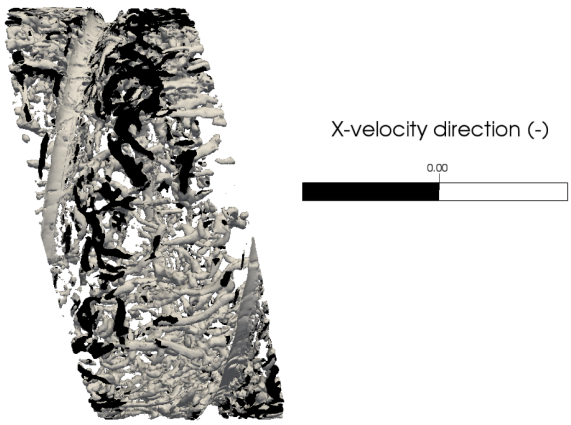

FIGURE 6. Instantaneous Q-criterion isosurface, colored in black and white by axial velocity direction. Black color correspond to the recirculating flow.

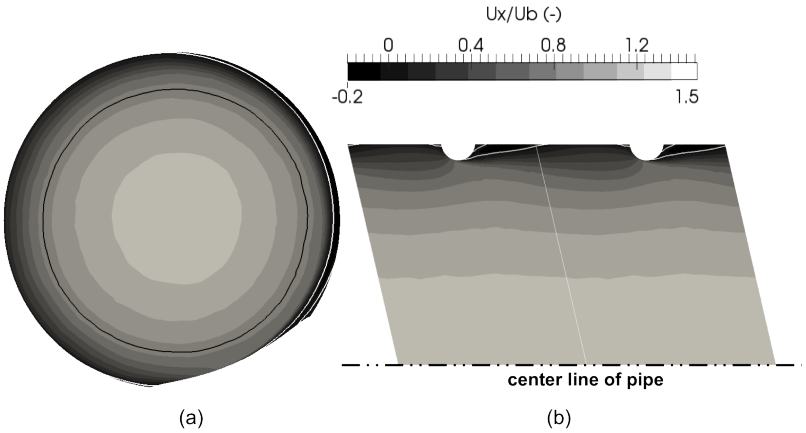

FIGURE 7. Mean axial velocity field normalized by u_b. (a) a transverse cut; (b) one half of an axial cut illustrated with two patterns, the dashed line indicates the center line of the pipe. The black line in (a) marks the axial velocity reaching 99% of bulk velocity, and the white line marks zero-axial velocity in (a) and (b).

behind the rib. The zero-axial velocity limit is marked with a white line, shows a small upstream recirculation zone and a longer downstream one, starting at the top of the rib and extending downstream over a distance of about $p/2$ (i.e. $4e$). This confirms the strongly separated wall flow and has a direct impact on wall friction. In addition, the flow accelerates on the top of the rib, resulting in a thinner boundary layer in this zone. Another remarkable feature of this flow is the rotating motion, illustrated in Figure 8. The rib geometry creates a non-zero azimuthal velocity that is maximum in the near-wall region and gradually decreases toward the center of the pipe. This rotating motion helps the flow to maintain axisymmetry and contributes to the pressure loss as it extracts energy from the imposed pressure gradient.

The effect of the ribs on the wall flow is shown in Figure 9 where time-averaged axial and azimuthal profiles are plotted at a series of locations along the pipe. The shape of the profiles differs mainly in the near wall region, while both axial and azimuthal velocity

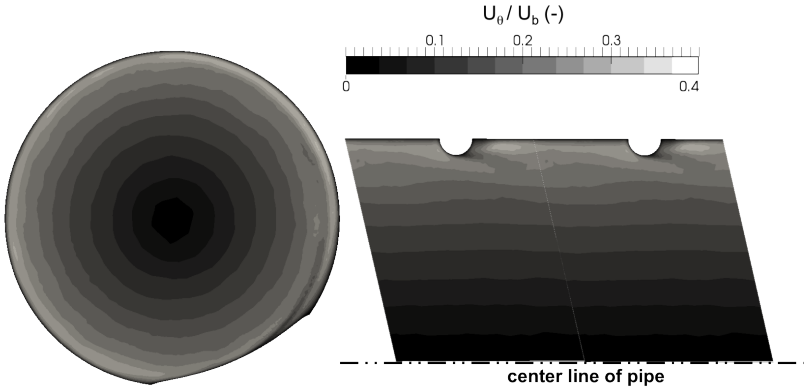

FIGURE 8. Mean azimuthal velocity field normalized by u_b. (a) a transverse cut; (b) one half of an axial cut illustrated with two patterns, the dashed line indicates the center line of the pipe.

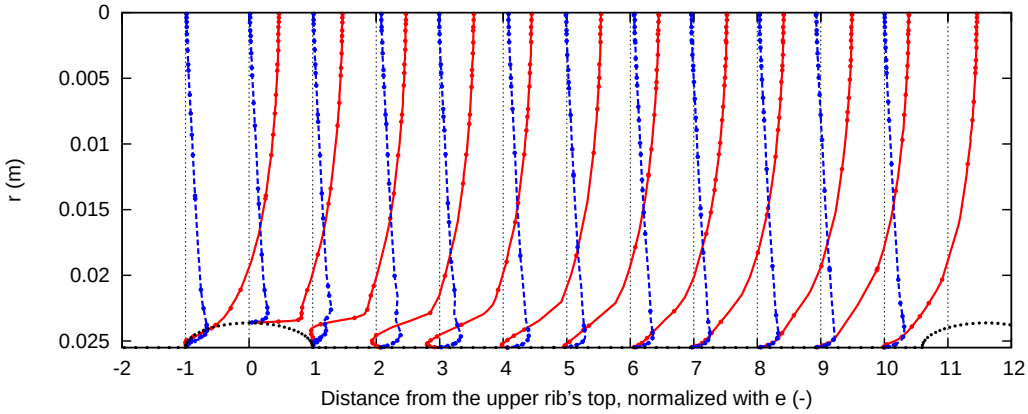

FIGURE 9. Time-averaged axial (——) and azimuthal (- - -) velocity profiles, normalized by the bulk axial velocity u_b, at various locations along the ribbed pipe. The value of normalized axial velocity on the central axis is 1.5 (the real value is equal to 92 m/s).

components stay unchanged on the central axis through the pipe, being respectively, $u_{cl}/u_b = 1.5$ (compared with 1.2 in a smooth pipe) and $w_{cl}/u_b = 0$. This confirms the limited blocking effect of the small-size ribs whose impact stays mostly confined to the wall region. The azimuthal velocity maintains a classical boundary layer behavior near the wall, whereas the axial velocity shows important variations near the wall due to the acceleration on the rib top and the recirculation zones. Such profiles may be useful for developing and testing wall models for LES of similar configurations.

Finally the impact of ribs on turbulence may be viewed from Figure 10, which shows the axial fluctuating velocity (rms). There is a clear trace of the rib, showing the turbulence production in the separation induced shear layer. The inter-rib distance is too large in this case to observe interaction between the turbulent wakes of two successive ribs, and there appears to be no cumulative effect in the axial direction. This is consistent with the observation that the simulation appears insensitive to the number of rib patterns involved. The zone of maximum turbulence intensity is maintained at a fixed wall distance

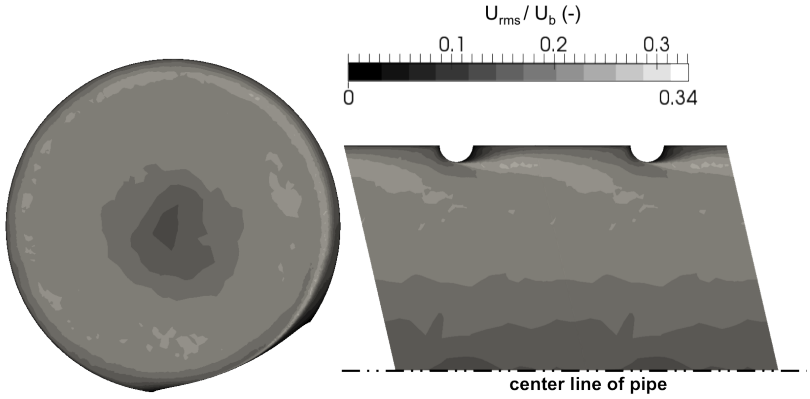

FIGURE 10. Axial fluctuating velocity field u_{rms} normalized by u_b. (a) a transverse cut; (b) one half of an axial cut illustrated with two patterns, the dashed line indicates the center line of the pipe.

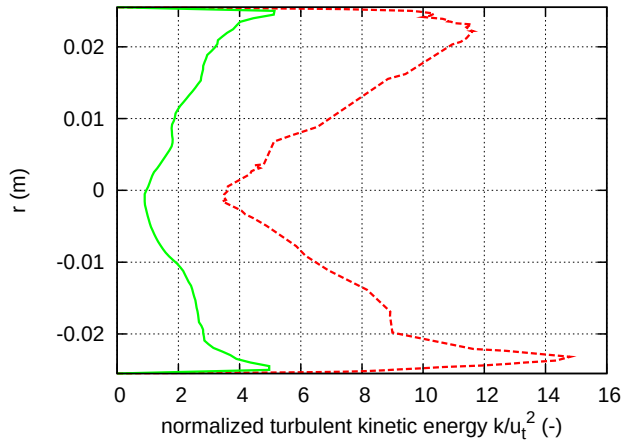

FIGURE 11. Time-avergaed profiles of turbulent kinetic energy (normalized by the friction velocity $u_\tau^2 = \tau_w/\rho$, where τ_w is the spatial mean shear stress) at location 9 of Figure 9 in both smooth (——) and ribbed (- - -) pipes.

corresponding to the rib top, which is therefore an important geometrical feature for maximizing mixing and enhancing of heating in the final application.

The difference with a smooth tube may be seen in Figure 11: profiles of normalized turbulent kinetic energy are plotted at location 9 of Figure 9 for both smooth and ribbed tubes. It appears that the turbulence intensity is significantly increased in the ribbed tube, with a turbulent mean kinetic energy level roughly three times larger. Consistent with the turbulent velocity fluctuations observed in Figure 10, the turbulence increase is highest close to the wall, in the rib wake, where the maximum kinetic energy is found there to be three times higher than the maximum kinetic energy in the smooth tube. Note that, contrary to the smooth tube case, the turbulent kinetic energy profile is not symmetric in the ribbed tube owing to the presence of the rib.

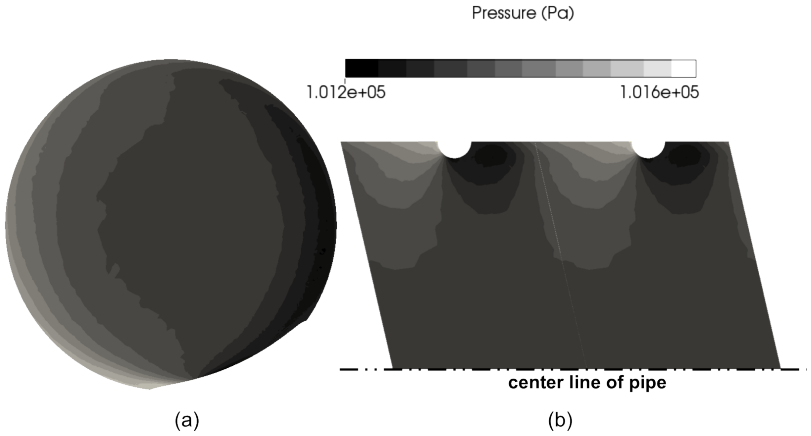

FIGURE 12. Mean pressure field. (a) a transverse cut; (b) one half of an axial cut illustrated with two patterns, the dashed line indicates the center line of the pipe.

3.2. *Shear stress and pressure loss*

The mean pressure field is shown in Figure 12 in the transverse and axial cut planes. Although the pressure increases in front of the rib and decreases behind, it stays undisturbed in the outer flow. These pressure variations are clearly correlated to the upstream and downstream recirculation zones and this knowledge could also be used in developing wall models. The pressure loss per unit length, normalized by $\rho u_b^2/2D$ is found to be 0.14, as estimated from the source term S_{qdm} necessary to maintain the flow. Compared with the normalized pressure loss of 0.021 in a smooth tube, this means an increased pressure loss of 550%, i.e. a significantly increased cost that must be compared with the possible gain in selectivity.

The Fanning friction factor here is equal to 0.035 (compared with 0.0053 in the smooth tube), much higher than all measured values for a Reynolds number of 28000 in Figure 2. This confirms that experimental correlations can not be used directly to estimate pressure loss in ribbed pipes and that accurate simulations and/or dedicated experiments are necessary.

To better understand this pressure loss, a balance equation is written for the axial momentum in steady flow

$$0 = \underbrace{-\oint P n_x dS}_{pressure\ \ drag} + \underbrace{\oint \vec{\tau}_x \cdot \vec{n} dS}_{friction\ \ drag} + \underbrace{\int S_{qdm} dV}_{total\ \ imposed\ \ force}, \tag{3.1}$$

where $\vec{n}$ is the wall surface normal vector and $\vec{\tau}_x = (\tau_{xx}, \tau_{xy}, \tau_{xz})$ is the axial stress vector. Figures 13 and 14 illustrate the evolution of the pressure coefficient C_p and the skin-friction coefficient C_f, defined as

$$C_p = \frac{P - P_{ref}}{1/2\rho u_b^2} \quad \text{and} \quad C_f = \frac{\vec{\tau}_x \cdot \vec{n}}{1/2\rho u_b^2}, \tag{3.2}$$

where the pressure in the downstream corner of the rib has been chosen as the reference P_{ref}, so C_p is equal to zero at this corner by the definition. On the other hand, C_p reaches a maximum value of 0.55 around the upstream corner of rib where recirculation zones are observed. The contribution of pressure Pn_x in Eq. (3.1) is non-zero only on the rib

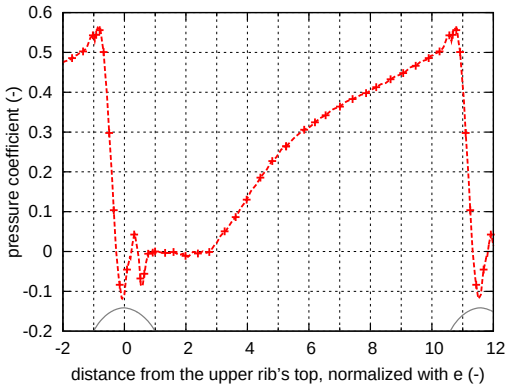

FIGURE 13. Evolution of the pressure coefficient C_p along the wall surface.

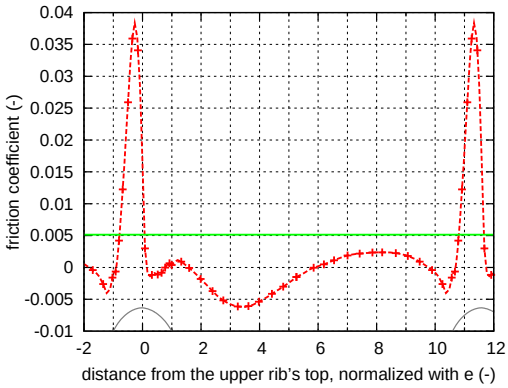

FIGURE 14. Evolution of the skin friction coefficient C_f along the wall surface. The solid line indicates the value for a smooth pipe.

	Pressure drag		Friction drag		Total drag	Total imposed force	
Ribbed tube	$1.26\ 10^{-1}$	(649%)	$5.24\ 10^{-3}$	(27%)	$1.31\ 10^{-1}$	$1.29\ 10^{-1}$	(665%)
Smooth tube	0	(0%)	$1.94\ 10^{-2}$	(100%)	$1.94\ 10^{-2}$	$1.94\ 10^{-2}$	(100%)

TABLE 1. Axial momentum equation balance in ribbed and smooth tubes. The calculated drag components and imposed force are all normalized by $\rho u_b^2 L^2$. Results are also expressed in percentage of the imposed source term in the smooth tube for a direct comparison between the ribbed and the smooth tube

surface, where $\vec{n}$ has a non-zero axial component. The wall shear stress exhibits a strong peak on the rib, with a maximum of $C_f = 0.0375$ ($\vec{\tau}_x \cdot \vec{n} = 27$ Pa), but becomes negative in the upstream and downstream recirculation zones. Between the ribs the wall shear stress is always below the smooth tube value represented by the solid line in Figure 14.

Table 1 gives the results of the axial momentum balance in the ribbed tube. For comparison purposes, results for a smooth tube are also reported.

Not surprisingly the total axial drag is mainly from the pressure drag created by the ribs. The flow separation induced by the ribs results in a contribution as high as 98% of the total drag from its pressure contribution. Consistently the friction force is reduced in comparison with the smooth case, because significant portions of the flow are detached. Flow separation and its effects regarding total drag provide some guidance for setup simulations of the same configuration at a reduced cost: (a) The flow separation is a critical feature that requires significant resolution to be accurately represented. Any under-resolved mesh in the vicinity of the wall would poorly capture this aspect and lead to inaccurate results regarding the total drag estimation. (b) This test case is a good candidate for roughness-type modeling in which an empirical sink term is added in the momentum equation, accounting for the local pressure loss created by the rib. This kind of modeling can potentially generate significant savings, especially regarding mesh generation as the computation would be carried out in a smooth tube. Modeling the pressure jump produced by the rib should help to recover the correct swirl properties

of the flow field by providing the correct torque. However, questions arise regarding the turbulence intensity level caused by the additional shear layer downstream the rib and should be tested in further studies.

4. Conclusions

LES of ribbed pipes with fully resolved boundary layer has been performed and has created an accurate database for the understanding and modeling of such flows. Results are of high interest for the targeted application of thermal cracking, as they fully describe mixing processes induced by the presence of the ribs. They also confirm that classical wall-laws can not describe the flow in such configurations and that accounting for flow separation is required. Next steps toward building the real system should include heat transfer and chemical processes, which are both strongly coupled to turbulence and require a similar approach.

Acknowledgments

This work was financed by TOTAL S.A. (France) and was performed using HPC resources from GENCI- [TGCC/CINES/IDRIS] (Grant 2014-x20142b5031).

REFERENCES

Bergles, A., Blumenkrantz, A. & Taborek, J. 1974 Performance evaluation criteria for enhanced heat transfer surfaces. *J. Heat Transfer* **2**, 239–243.

Colin, O. & Rudgyard, M. 2000 Development of high-order taylor-galerkin schemes for les. *J. Comput. Phys.* **162**, 338–371.

Ducros, F., Nicoud, F. & Poinsot, T. 1999 Subgrid-scale stress modelling based on the square of the velocity gradient tensor. *Flow Turbul. Combust.* **62**, 183–200.

García, A., Solano, J., Vicente, P. & Viedma, A. 2012 The influence of artificial roughness shape on heat transfer enhancement: Corrugated tubes, dimpled tubes and wire coils. *Appl. Therm. Eng.* **35**, 196–201.

Perry, A. E., Schofield, W. H. & Joubert, P. N. 1969 Rough wall turbulent boundary layers. *J. Fluid Mech.* **37**, 383–413.

Saha, S. 2010 Thermal and friction characteristics of turbulent flow through rectangular and square ducts with transverse ribs and wire-coil inserts. *Exp. Therm. Fluid Sci.* **34**, 575–589.

Sethumadhavan, R. & Raja Rao, M. 1983 Turbulent flow heat transfer and fluid friction in helical-wire-coil-inserted tubes. *Int. J. Heat Mass Transfer* **26**, 1833–1845.

Tani, I. 1987 *Turbulent boundary layer development over rough surfaces.* In: Perspectives in Turbulence Studies, pp. 223–249. Springer.

Zhang, Y. F., Li, F. Y. & Liang, Z. M. 1991 *Heat transfer in spiral-coil-inserted tubes and its application.* In: Advances in Heat Transfer Augmention, MA Ebadin, DW Pepper and T. Diller, Eds., ASME Symp. Vol. HTD, vol. 169, pp. 31–36.